COST COMPETITIVE STEEL FIBER REINFORCED SELF-COMPACTING CONCRETE FOR STRUCTURAL APPLICATIONS

Joaquim A. O. Barros [1], Lúcio A. P. Lourenço [2], Rajendra K. Varma[3], Delfina M. F. Gonçalves[4]

Abstract: The present work resumes the research carried out to develop a cost competitive Steel Fibre Reinforced Self-Compacting Concrete (SFRSCC) for structural applications, such is the case of lightweight panels for building facades. A mix design method was developed taking into account the influence that fibres introduce in the skeleton phase of the composition. The concrete precast industry is one of the most suited industries for the use of SFRSCC, due to the possibility of assuring high levels of quality control from the mix composition phase up to the curing process of the manufactured structural elements. Since demoulding of the precast elements should be executed as earliest as possible, due to economic and stock management reasons, the influence of age on the SFRSCC mechanical properties was assessed carrying out compression and flexural tests. Compression and monotonic cyclic tests were also carried out to assess the predictive performance of analytical formulations. To appraise the structural possibilities of the developed SFRSCC, panel prototypes were subject to flexural and punching load configurations. The obtained results showed the great benefits provided by the fibre reinforcement mechanisms. Finally, a real scale panel was constructed and tested in an industrial environment, in order to help in the establishment of the best practices of technology transfer from laboratory to factory, as well as to determine the load carrying capacity of this type of structural elements.

KEYWORDS: Self-compacting concrete; Steel fibres; Compression; Flexural; Punching; Real scale test.

[1] Associate Professor, Dept. of Civil Engineering, Univ. of Minho, Campus de Azurém, 4810-058 Guimarães, Portugal.
E-mail: barros@civil.uminho.pt *Corresponding author*
[2] PhD Student, Dept. of Civil Engineering, Univ. of Minho, Campus de Azurém, 4810-058 Guimarães, Portugal.
E-mail: lucio@civil.uminho.pt;
[3] PhD Student, Dept. of Civil Engineering, Univ. of Minho, Campus de Azurém, 4810-058 Guimarães, Portugal
E-mail: rajendra@civil.uminho.pt
[4] Researcher, Civitest Company, 2ª Fase, Lote S6, 4705-414 Celeirós, Braga, Portugal
E-mail: fina@civitest.pt

1 - INTRODUCTION

The concrete precast industry is frequently confronted with the production of structural reinforced concrete elements of some complex geometry. These geometric conditions introduce difficulties on the placement of reinforcement, resulting in a large consuming time during the industrial process. Moreover, when high percentage of reinforcement is used, there are difficulties on assuring the desired concrete pouring quality, resulting in deficiencies that can compromise the mechanical behaviour and the visual appearance of the final structure.

Self-Compacting Concrete (SCC) can be defined as a concrete that is able to flow in the interior of the formwork, filling it in a natural manner and passing through the reinforcing bars and other obstacles, flowing and consolidating under the action of its own weight (Okamura 1997).

Short and randomly distributed steel fibres are often used to reinforce cementitious materials, since they offer resistance to crack initiation and, mainly, to crack propagation. In steel fibre reinforced concrete (SFRC) of low fibre volume fraction the principal benefits of the fibres appear after matrix cracking has occurred, since fibres crossing the crack guarantee a certain level of stress transfer between both faces of the crack, providing to the composite a residual strength, whose magnitude depends on the fibre, matrix and fibre-matrix properties. The mechanical performance of SFRC is highly influenced by the fibre dispersion, since the effectiveness of fibres depend on how the fibres are oriented, their location and arrangement within the cement matrix.

The advantages associated to the addition of steel fibres to concrete mixes may be joined with the ones resulting from the self-compacting ability concept in concrete, with the formulation of steel fibre reinforced concrete mixes exhibiting self-compacting ability. The resulting material is, in this work, designated by Steel Fibre Reinforced Self Compacting Concrete (SFRSCC).

In the ambit of the present applied research project, a lightweight SFRSCC panel system was developed. At the material age of one day, this SFRSCC should have an average compressive strength greater than 20 MPa and an equivalent flexural tensile strength (Barros *et al.* 2005) greater than 3 MPa. For reasons of economic viability, these values should be attained with a cement content not exceeding 400 kg per concrete m^3 with no addition of silica fume. When compared to the solutions currently used, this SFRSCC has some advantages, such as: higher productivity and healthier labour conditions; initial and long term larger toughness; better quality control of the final products; lower costs (Barros *et al.* 2005).

In the present work, the procedure followed to develop a cost effective and high performance SFRSCC is briefly described. The hardened SFRSCC performance in terms of material and structural behaviour at early ages is

assessed. Compression and flexural tests were carried out with the objective of showing that it is possible to formulate relatively low-cost SFRSCC mixes, exhibiting good mechanical behaviour and other relevant properties for structural applications. Monotonic and cyclic compression tests also have the purpose of appraising the performance of proposed analytical models.

When installed, the flexural resistance of the panels is the principal design consideration since the bending moments that result from wind loading cause the greatest influence on the most unfavourable load combination. To assess the panel flexural behaviour, representative SFRSCC panel prototypes were tested. Since the SFRSCC layer at the lightweight parts of the panel is only 30 mm thick, its resistance to punching was also determined from experimental tests.

A real scale panel was fabricated and tested in a precast factory to assess the influence, in terms of material and structural performance, of eventual difficulties that can be found when the laboratory routines are adjusted for the production of prototypes in an industrial environment. The test results demonstrated the structural potential of the developed cost competitive SFRSCC.

2- MIX DESIGN METHOD

The materials used were cement (C) CEM I 42.5R (rapid hardening and high strength cement, according to EN197-1:2000, limestone filler (LF), a third generation superplasticizer (SP) based on polycarboxilates (Glenium® 77 SCC), water (W), three types of aggregates (fine river sand (FS), coarse river sand (CS) and crushed granite 5-12 mm (CG)) and DRAMIX® RC-80/60-BN hooked end steel fibres. This fibre has a length (l_f) of 60 mm, a diameter (d_f) of 0.75 mm, an aspect ratio (l_f/d_f) of 80 and a yield stress of 1100 MPa.

The methodology followed to formulate SFRSCC compositions is mainly based on the following three steps: i) the proportions of the constituent materials of the binder paste are defined; ii) the proportions of each aggregate on the final granular skeleton are determined; iii) binder paste and granular skeleton are mixed in distinct proportions until self-compacting requirements in terms of spread ability, correct flow velocity, filling ability, blockage and segregation resistance are assured, allowing the determination of the optimum paste content in concrete. A detailed description of the method can be found elsewhere (Pereira 2006). Table 1 includes two developed SFRSCC compositions (the amount of water referred does not include the aggregate's saturation water). The first one was used to assess the influence of the age on both the compressive strength and Young's Modulus of the SFRSCC. This SFRSCC was also used to evaluate the punching and the flexural behaviour of panel prototype. The second composition was used to appraise the performance of a monotonic and a cyclic

analytical model for the simulation of the SFRSCC compression behaviour when subject to monotonic and cyclic compressive loading, respectively. For both compositions, the total spread, *s*, and the time to reach a spread diameter of 500 mm, T_{50}, were measured (EFNARC 2002). In the second composition, the T_{20}, T_{40} and H_2/H_1 parameters of the L Box test were also measured (EFNARC 2002). For the developed compositions, no visual sign of segregation was detected and the mixtures showed good homogeneity and cohesion, even while flowing trough the smaller orifice of the Abrams cone (while testing, the Abrams cone was always used in the inverted position).

3 – TESTS WITH STANDARD SPECIMENS

The performance evaluation of the designed SFRSCC was based on the assessment of the compression and flexural behaviour of hardened SFRSCC. Cylinder specimens of 150 mm diameter and 300 mm height, and prismatic specimens of 600×150×150 mm^3 were moulded without any externally applied compaction energy, for the compression and flexural tests, respectively.

3.1 – Compression Tests

3.1.1 Equipment and test set up

The procedures adopted for the assessment of the axial stress-strain relationship of the SFRSCC cylinder specimens were in accordance with the recommendations of ASTM C 39 - 96 (1996). Each test was carried out in a servo-controlled test machine, with a load carrying capacity of 3000 kN. The test control procedure was defined using the axial displacement as control variable, measured by the internal displacement transducer installed inside the loading equipment. The imposed axial displacement rate ($\dot{u}$) was 5 μm/s in the monotonic tests, while in the cyclic tests the $\dot{u}$ was 30 μm/s for the strain ranges 0‰-2‰ and 8‰-10‰, and 15 μm/s in the strain range 2‰-8‰: The results were obtained from three external displacement transducers disposed at 120º around the specimen, registering the displacement between the two opposite steel load platens. The axial displacement was computed from these results, and then divided by the specimen's initial height to obtain the axial strain.

The procedures followed to assess the modulus of elasticity (E_c) of the SFRSCC specimens were mainly based on RILEM TC14-CPC8 (1975), and on ASTM C 469 - 94 (1994). The tests were carried out in the same equipment used to obtain the compression stress-strain relationships. The test control procedure was defined

using the axial load as control variable, measured by the internal load cell included on the upper plate of the loading equipment. The prescribed loading sequence consisted on three loading-unloading cycles, with the load value varying between an upper level of one third of the estimated compressive strength at each age, and the lower level of 0.5 MPa. The final value of the elasticity modulus was obtained for each specimen by dividing the stress difference between loading and unloading cycles, by the strain difference observed in the last unloading cycle.

3.1.2 – Influence of the SFRSCC age on its compressive strength and Young's Modulus

The developed SFRSCC, corresponding to the mix composition nº 1 (Table 1), was used to assess the influence of the SFRSCC age on its compressive strength and Young's Modulus. For this purpose, compression tests were carried out at 5 distinct ages: 12 and 24 hours, 3, 7 and 28 days. The resulted axial stress-strain curves, represented in Fig. 1, correspond to the average load values observed at each strain level, obtained from three specimens at each age. Observing the results presented in this figure, the improvement of the post-cracking compression behaviour is apparent at all ages, having in mind the typical shape of the compression axial stress-strain curves for plain concrete (CEB-FIP 1993). Steel fibres, mainly the ones disposed at a perpendicular direction with respect to the longitudinal cylinder axis, bridge longitudinal cracks and the eventual major inclined crack emerging when the peak load is reached. These additional resisting mechanisms oppose to damage propagation and delay the after peak loss of load carrying capacity. The post-peak load sustaining capacity assured by fibre reinforcement has, however, decreased with the age. This reduction becomes more evident for the ages of 7 days and 28 days. Despite presenting greater peak loads, the specimens tested at 7 days and 28 days ages reveal smaller residual strengths than the younger specimens for greater deformations. This behaviour may be interpreted as an indicator of the increase in brittleness of concrete matrices with the increase of strength, associated to a reduction of the stress redistribution capacity and the consequent concentration of deformation in a smaller number of cracks, which have decreased the fibre reinforcement effectiveness. Furthermore, the energy released at crack initiation is as high as strong is the matrix. To sustain this energy in a stable fashion, the number of fibres bridging the cracks should accompany the resistance of the matrix. Since the content of fibres, in this series of tests, remained constant, the load supported by each fibre crossing a crack increased with age, due to the matrix strength increase. For the 7 and 28 days specimens, steel fibres seem to be less efficient on sustaining the specimen load carrying capacity in the post peak stage. This suggests that the load

transferred to the fibres at matrix crack initiation over passed a load limit, beyond which the fibre-matrix pullout bond strength mechanisms are affected and their efficacy is reduced.

Referring to the compressive strength evolution in time, Fig. 2a shows a very fast strength gaining occurred with the age, with an average compressive strength of 25 MPa at 12 hours. Taking as reference value the compressive strength at 28 days, the compressive strength evolution at early ages was estimated based on the equation recommended by CEB-FIP Model Code (1993). In Fig. 2a the compressive strength evolution predicted by CEB-FIP equation is compared with the experimental results. In fact, it is apparent that a pronounced compressive strength increase occurs at very early ages. This rapid early age strength gaining might be associated to the type of cement used. However, this factor was already taken into account on the estimation of the strength gaining evolution by CEB-FIP equations. Another two factors that may be the origin of this rapid early strength gaining are the reduced water amount used in the mix and the introduction of large amounts of limestone micro-filler. These two factors, together, may be the cause for the establishment of stronger interactions between the small particles in solution composing the paste, due to an increase of the proximity between them. As a consequence, the dynamics of the chemical reactions in solution may be changed. Other studies seem to agree on this assumption (Poppe and Shutter 2005).

The average values of the elasticity modulus, obtained at each age, and the scatter of the corresponding results are depicted in Fig. 2b. As a reference, the elasticity modulus was estimated for plain concrete at each age based on the CEB-FIP equations, using the results obtained for compressive strength and admitting the granitic nature of the aggregates. When compared to the experimental results, Fig. 2b shows that both curves present a similar shape, but the magnitude of values is clearly different. The SFRSCC showed higher deformability than expected for a conventional plain concrete mix, at all tested ages. The main reason for the greater deformability observed in SFRSCC may reside on the much greater paste contents typically present in self-compacting concrete mixes than in the conventional concretes. Since aggregates are much less deformable than hardened paste, in a hardened composition with higher paste contents the deformability is obviously higher (van Mier 1984). The values of the compressive strength and the elasticity modulus of each carried test are referred elsewhere (Pereira 2006).

3.1.3 – Models for the simulation of the monotonic and cyclic compression behaviour

To evaluate the compressive cyclic behaviour of SFRSCC, another experimental program was carried out with the specimens moulded from the mix composition nº 2 (Table 1). The data derived from this experimental

program will be used to appraise a constitutive model to simulate the cyclic compressive behaviour of the developed SFRSCC and to verify the applicability of a compressive envelope equation previously proposed for steel fibre reinforced concrete (SFRC) (Barros and Figueiras 1999). This experimental program is composed of nine specimens, six of them were tested under cyclic compressive loading, while the remaining three specimens were tested under monotonic loading, at the age of 14 days. At this age, the developed SFRSCC presented an average value for the Young's Modulus and compressive strength of 36 GPa and 55 MPa, respectively. Fig. 3 shows typical cyclic and monotonic stress-strain curves obtained in this experimental program, where it is evident that the monotonic curve corresponds to the envelope of the cyclic curve.

For modelling the monotonic compressive behaviour the following equation is proposed (in this subsection the strains and the stresses are considered with negative signal):

$$\sigma_c = f_c \frac{\frac{\varepsilon_c}{\varepsilon_{c1}}}{(1-p-q)+q\left(\frac{\varepsilon_c}{\varepsilon_{c1}}\right)+p\left(\frac{\varepsilon_c}{\varepsilon_{c1}}\right)^{\frac{1-q}{p}}} \tag{1}$$

with

$$q = 1-p-\frac{E_{c1}}{E_{ci}}, \quad p+q \in]0,1[, \quad \frac{1-q}{p} > 0 \tag{2}$$

where f_c is the compressive strength, ε_{c1} its corresponding strain, E_{c1}/E_{ci} is the ratio between the secant modulus of elasticity ($E_{c1} = f_c/\varepsilon_{c1}$) and the tangent modulus of elasticity (E_{ci}). The parameter p is obtained by minimizing the following equation:

$$e^2 = \sum_{i=1}^{n}\left(\frac{\sigma_{ci}^r - \sigma_{ci}^c}{f_c}\right)^2 \tag{3}$$

where σ_{ci}^r and σ_{ci}^c are the stresses obtained in the experiments and calculated from expression (1), respectively, and n is the number of scan readings in a test. Using this strategy, and considering for the E_{ci}, f_c and ε_{c1} the average values registered in the monotonic tests, it was verified that p=0.25 led to the best fitting of the experimental results (see Fig. 4). However, to turn general this methodology, the p factor should be estimated based on the main parameters that influence the compression post-peak behaviour of a FRC, namely: the geometrical and material characteristics of the fibres, the fibre content, the characteristics of the concrete matrix. This research will be executed in a next future, in the ambit of the present research project.

The model adopted to simulate the compression hysteretic behaviour of SFRSCC is schematically represented in Fig. 5. A general hysteretic scheme is simulated by the paths $\overline{BC}$, $\overline{CD}$, $\overline{DE}$, $\overline{EF}$ and $\overline{FG}$. These paths are simulated by the following equations:

$$\sigma_c = \bar{\sigma}_c^{\min}\left(\frac{\varepsilon_c - \varepsilon_c^{pl}}{\bar{\varepsilon}_c^{\min} - \varepsilon_c^{pl}}\right)^a \quad if \quad \begin{cases} \varepsilon_{cu} < \varepsilon_c^{\min} \le 0 \\ \varepsilon_c^{\min} < \varepsilon_c \le \varepsilon_c^{pl} \\ \Delta\varepsilon_c > 0 \end{cases} \tag{4.1}$$

$$\sigma_c = \bar{\sigma}_c^{\min}\left(\frac{\varepsilon_c - \varepsilon_c^{pl}}{\bar{\varepsilon}_c^{\min} - \varepsilon_c^{pl}}\right)^a \quad if \quad \begin{cases} \varepsilon_{cu} < \varepsilon_c^{\min} \le \varepsilon_c^{e} \\ \varepsilon_c^{\min} < \varepsilon_c \le \varepsilon_c^{pl} \ (\overline{BC} \text{ and } \overline{DE}) \\ \Delta\varepsilon_c > 0 \end{cases}$$

$$\sigma_c = \sigma_{c(pf)}^{urc} + \left(\bar{\sigma}_c^{\min} - \sigma_{c(pf)}^{urc}\right)\left(\frac{\varepsilon_c - \varepsilon_{c(pf)}^{urc}}{\bar{\varepsilon}_c^{\min} - \varepsilon_{c(pf)}^{urc}}\right) \quad if \quad \begin{cases} \varepsilon_{cu} < \varepsilon_c^{\min} \le 0 \\ \varepsilon_c^{\min} < \varepsilon_c \le \varepsilon_c^{pl} \ (\overline{CD} \text{ and } \overline{EF}) \\ \Delta\varepsilon_c \le 0 \end{cases} \tag{4.2}$$

$$\sigma_c = \sigma_{cf}^{rec} + E_{c,env}^{rec}\left(\varepsilon_c - \varepsilon_{cf}^{rec}\right) + b\left(\varepsilon_c - \varepsilon_{cf}^{rec}\right)^2 \quad if \quad \begin{cases} \varepsilon_{cu} < \varepsilon_c^{\min} \le 0 \\ \varepsilon_{cf}^{rec} < \varepsilon_c \le \varepsilon_c^{\min} \ (\overline{FG}) \\ \Delta\varepsilon_c \le 0 \end{cases} \tag{4.3}$$

The monotonic branches $\overline{OB}$ and $\overline{GH}$ are simulated by the monotonic stress-strain relationship of Eq. (1). Eq. (4.1) simulates the paths $\overline{BC}$ and $\overline{DE}$, i.e., both the partial and full unloading branches. In case of $\overline{BC}$ $\bar{\varepsilon}_c^{\min} = \varepsilon_{cons}^{unl}$ is the strain at point B, at the onset of unloading, and $\bar{\sigma}_c^{\min} = \sigma_{cons}^{unl}$ its corresponding stress, while at the case of $\overline{DE}$, $\bar{\varepsilon}_c^{\min} = \varepsilon_{cp}^{ruc}$ and $\bar{\sigma}_c^{\min} = \sigma_{cp}^{ruc}$, which is evaluated from the following equation:

$$\sigma_{cp}^{ruc} = \sigma_{cp}^{urc} + \left(\frac{\sigma_{cf}^{rel} - \sigma_{cp}^{urc}}{\varepsilon_c^{\min} - \varepsilon_{cp}^{urc}}\right)\left(\varepsilon_{cp}^{ruc} - \varepsilon_{cp}^{urc}\right) \tag{5}$$

where

$$\sigma_{cf}^{rel} = 0.92\,\sigma_{cons}^{unl} + 0.08\,\sigma_{cp}^{urc} \tag{6}$$

which is responsible for modelling the degradation in the compressive reloading stiffness. In Eq. (4.1) ε_c^{pl} is the compressive plastic strain that, according to Okamura and Maekawa (1991) can be evaluated from the following equation:

$$\varepsilon_c^{pl} = \varepsilon_c^{\min} - \frac{20}{7}\left[1 - \exp\left(-0.35\,\frac{\varepsilon_c^{\min}}{\varepsilon_{c1}}\right)\right]\varepsilon_{c1} \tag{7}$$

The *a* shape factor of Eq. (4.1) can be determined from the equation proposed by Wang *et al.* (1981):

$$a = 1.0 + 0.7\left(\frac{\varepsilon_c^{\min}}{\varepsilon_{c1}}\right) \tag{8}$$

Eq. (4.2) simulates the paths $\overline{CD}$ and $\overline{EF}$, i.e., the partial reloading and the reloading up to the experienced minimum compressive strain (ε_{cons}^{unl}). For the partial reloading, branch $\overline{CD}$, $\varepsilon_{c(pf)}^{urc} = \varepsilon_{cp}^{urc}$ and $\sigma_{c(pf)}^{urc} = \sigma_{cp}^{urc}$ are the strain and the stress at point C. For this branch, $\overline{\varepsilon}_c^{\min} = \varepsilon_{cons}^{unl}$ and $\overline{\sigma}_c^{\min} = \sigma_{cp}^{ruc}$, where σ_{cp}^{ruc} is calculated from Eqs. (5) and (6). In the case of the branch $\overline{EF}$, $\varepsilon_{c(pf)}^{urc} = \varepsilon_{cf}^{urc} = \varepsilon_c^{pl}$, $\sigma_{c(pf)}^{urc} = \sigma_{cf}^{urc} = 0$, $\overline{\varepsilon}_c^{\min} = \varepsilon_{cp}^{ruc}$ and $\overline{\sigma}_c^{\min} = \sigma_{cp}^{ruc}$, with σ_{cp}^{ruc} calculated from Eqs. (5) and (6).

The strain of the returning point G on the compressive envelope curve can be obtained from the following equation:

$$\varepsilon_{cf}^{rec} = \varepsilon_{cons}^{unl} + \frac{4}{3}\left(\frac{\sigma_{cons}^{unl} - \sigma_{cf}^{rel}}{\sigma_{cf}^{rel}}\right)\left(\varepsilon_{cons}^{unl} - \varepsilon_c^{pl}\right) \tag{9}$$

and the corresponding stress, σ_{cf}^{rec}, is determined replacing ε_c by ε_{cf}^{rec} in Eq. (1).

Finally, Eq. (4.3) simulates the path $\overline{FG}$, i.e., the returning to the envelop curve, where

$$E_{c,env}^{rec} = \left.\frac{d\sigma}{d\varepsilon}\right|_{\varepsilon=\varepsilon_{cf}^{rec}}^{env} \tag{10}$$

is the tangent to the envelope curve (Eq. (1)), evaluated at the strain ε_{cf}^{rec}, and *b* factor is determined from:

$$b = \frac{\sigma_{cf}^{rel} - \sigma_{cf}^{rec} - E_{c,env}^{rec}\left(\varepsilon_{cons}^{unl} - \varepsilon_{cf}^{rec}\right)}{\left(\varepsilon_{cons}^{unl} - \varepsilon_{cf}^{rec}\right)^2} \tag{11}$$

This model was applied to the simulation of the cyclic compression tests. The comparison is presented in Fig. 6, from which it can be concluded that the model simulates with high accuracy the compression cyclic behaviour of SFRSCC specimens.

3.2 - Flexural Behaviour

The developed SFRSCC, corresponding to the mix composition nº 1 (Table 1), was used to assess the influence of the SFRSCC age on its flexural behaviour. For this purpose, simply supported notched beams were tested under three-point loading conditions, according to the recommendations of RILEM TC 162-TDF (2002). Four prismatic specimens of 150 × 150 mm^2 cross section and a length of 600 mm were tested at each of the five studied ages. The notch at midspan was produced on one of the faces perpendicular to the casting surface, using wet sawing. The width of the notch was 3 mm, and the depth 25 mm, leaving a section with a net depth (h_{sp}) of 125 mm at midspan. The distance between the two roller supports was 500 mm, and the deflection was measured at midspan with a displacement transducer.

The tests were carried out with closed-loop testing equipment, using the deflection at midspan for test control purposes. After reaching a midspan deflection of 0.1 mm, the displacement rate was increased to 3 μm/s. The test was stopped when a total deflection at midspan of 3 mm was reached. The smaller deflection rate imposed to the specimen at the beginning of the testing sequence had the purpose of avoiding test instabilities due to crack initiation at the matrix. The results obtained at each of the five testing ages are represented in Fig. 7. Each curve represents the average load at each midspan deflection, measured in 4 specimens at each age. It can be observed that, as a result of the tensile strength increase of concrete matrix with age, the load at the limit of proportionality (F_L), corresponding to the maximum load reached up to a deflection of 0.05 mm (Vandewalle *et al.* 2002), clearly increased with age. In a following stage, for deflections between 0.05 mm and 0.2 mm, a slight decay of the load carrying capacity occurs for all ages, but this reduction assumes greater relevance with age. At this stage, the equilibrium at the onset of matrix cracking is achieved by the migration of the tensile stresses from concrete matrix to the steel fibres. Since the concrete matrix tensile strength increases with its age, the fibres need to sustain an increase tensile stress resultant. In consequence, the force transferred to each steel fibre increases with concrete age because a constant amount of steel fibres was used for all ages, which justifies the observed increasing load decay with the age, at this stage. After this transition stage has been overcome, a new stage of increasing load carrying capacity is observed at all ages, for deflections greater than 0.2 mm, due to an effective contribution of steel fibres for the toughening mechanisms in concrete matrix. An exception is found, though, at the 28 days age, exhibiting the load-deflection curve a very slight strength increase when compared to the other curves, followed by pronounced load decay. Starting at an approximate deflection of 1.0 mm, this load decay gradually leads to an intersection with all the other 4 curves, ending at a deflection of 3 mm with a much lower residual strength than any other. The increase on tensile strength of the concrete matrix with the age is probably, once more, the main reason justifying these results. For the 28 days specimens, due to the transference

of a significant load from matrix to fibres at the onset of matrix cracking, damages occur on fibre-matrix bond mechanisms, irremediably affecting the toughness efficacy provided by steel fibres. For this level of transferred load, the number of fibres for this composition (30 kg/m^3) seems to be insufficient to guarantee a fibre slip below the slip at fibre peak pull-out force, i.e., in the ascending branch of the fibre-matrix bond stress-slip relationship, τ_f-s_f (Robins *et al.* 2002). As a result, the steel fibres located just above the notch entered in the softening phase of the τ_f-s_f behaviour, conferring a flexural softening behaviour to the notched beams.

For the tested specimens, the values of the parameters proposed by RILEM TC 162-TDF (2002) to define the flexural behaviour of SFRC can be found elsewhere (Pereira 2006)

4 - STRUCTURAL BEHAVIOR

4.1 - Introduction

As already mentioned, steel fibre reinforcement is particularly efficient in structures with redundant number of supports, since high stress redistribution occurs after concrete crack initiation. In this context, SFRSCC panel prototypes were tested under punching and bending setup conditions, allowing the evaluation of the SFRSCC behaviour under the two most demanding loading conditions for the facade panels. The panel prototypes were fabricated by the SFRSCC composition nº 1, indicated in Table 1. The punching tests were executed in panel prototypes of 600 × 600 mm^2 and 110 mm thick, and the flexural tests were carried out in panel prototypes of 1000 × 1000 mm^2 and the same thickness, both at an age of 7 days.

4.2 - Punching Test on Panel Prototype

As represented in Fig. 8a, the lightweight central region of the panel prototype subjected to punching load is composed of a concrete layer of 30 mm thick. The procedure followed to assess the load-deflection behaviour of the lightweight SFRSCC panel prototype consisted on applying a load at the centre of the panel, by means of a square steel plate of 100 mm edge and 10 mm thick. The loading sequence was executed using the vertical displacement as control variable, measured by the internal displacement transducer included on the loading equipment. A vertical displacement rate of 25 μm/s was prescribed, and the testing procedure was stopped when punching failure was observed. The results obtained in terms of load-deflection curve are represented in Fig. 8b. After a short linear elastic phase, the panel entered into an elastic-cracked phase and supported an increasing load up to 40 kN. This load level was then maintained practically constant from a deflection of 1.4 mm up to a deflection of about 3 mm, representing 1% of the lightweight zone span. Then, the load suddenly fell from the

40 kN to approximately 20 kN, suggesting the occurrence of failure by punching. Fibres bridging the surfaces of the punching failure crack offered some resistance to the opening of this crack, delaying the loss of contribution of the aggregate interlock for the punching resistance. This justifies the relatively high level of residual strength that decreases very slowly with the deflection increase. The estimation of the steel fibres contribution for punching strength increase is further discussed in the section dedicated to the numerical simulation of these tests.

4.3 - Flexural Test in Panel Prototype

The panel prototype destined for the evaluation of flexural behaviour was conceived using the same lightweight concept as in punching. As represented in Fig. 9a, lightweight zones had also a concrete upper layer of 30 mm thick, and the thicker zones of the panel constituted a grid system of two-per-two orthogonal ribs. The panel has also a contour rib of 100 mm width. The test procedure consisted of applying a constant displacement rate (25 μm/s) at the centre of a main loading steel beam, connected to other two transversal secondary beams by means of two rollers. Load was transmitted to the four loading points at rib intersections by means of four square steel plates (100×100×20 mm^3) and four steel spheres of 20 mm diameter, in contact with the ends of the secondary loading beams. This entire loading mechanism was idealized with the intention of assuring that, independently of the observed deflection beneath each of the four loading points, the applied load was the same in each loaded area. To obtain the vertical deflection beneath each of these four loaded areas, four displacement transducers were there installed. The supports system was constituted by eight elements placed at the ends of the grid ribs. Each of these elements was constituted by a steel plate (100×100×10 mm^3) in contact with the bottom surface of the panel, and a steel sphere of 20 mm diameter, placed between the steel plate and the ground, guaranteeing that only the vertical displacement was constrained (lifting was not prevented). The results obtained in terms of load-deflection curve are represented in Fig. 9b, showing that the load retaining capacity of the structure assumes relevance, in similitude to the results observed at punching tests. To simplify the analysis, only the average results will be considered. After reaching a peak load of approximately 55 kN, the panel demonstrates the ability to almost totally retain the load carrying capacity up to an average deflection of around 5 mm. Even then, the load carrying capacity decreases very slowly with the increase of the average deflection increase, and the test sequence is stopped for a load of 15 kN (27% of the peak load) due to excess of deformation and incompatibility with the supports and the loading apparatus.

5 – TESTING A REAL SCALE SFRSCC PANEL

With the aim of verifying if the procedures adopted in the laboratory, in the development of a SFRSCC, can be directly applicable in industrial environment, the real scale SFRSCC panel, represented in Fig. 10, was fabricated and tested in a precast company. The test has also the purpose of evaluating the behaviour of a real panel when submitted to its dead weight and to an increase live load up to its rupture.

Two mixtures of 400 dm^3 were made to fabricate the panel. Both concrete mixtures were stable without any indication of segregation. The spread was 600 mm and 630 mm in the mixtures 1 and 2, respectively, while the H2/H1 parameter of the L-Box test was 0.80 (the test was only carried out for the second mixture). The demolding of the panel was done in the day after it had been casted, when the SFRSCC had an age of 24 hours. The panel was demolded almost in vertical position. After that, the panel was placed in a support until the test, which occurred at 7 days of panel age. Fig. 11 represents the panel support conditions and the location where the deflection was measured (centre of the panel). The panel was supported in four points. To simulate a uniform distributed live load, concrete plates of 500×500 mm^2, each one of 25 kg, were uniformly distributed in the area interior to the panel supports (Fig. 12). The panel supported 33 concrete plates, corresponding to a uniform distributed load of 8.25/(3.1×1.5)=1.77 kN/m^2, plus its dead weight (1.47 kN/m^2). When placing the 33rd concrete plate, an abrupt increase of deflection occurred, having the test been interrupted due to safety reasons (Fig. 12). When the 18th concrete plate was placed, a deflection of 24 mm was measured. When the test was interrupted, the deflection was about 44 mm and the maximum crack opening of the critical crack was around 3 mm. Fibres crossing this crack were visible. The overload of 1.77 kN/m^2 is higher than the characteristic value of the wind dynamic pressure that actuates in the major part of buildings where facade panels can be applied.

7 - CONCLUSIONS

In the present work an innovative mix design method was proposed to develop cost competitive and high performance steel fibre reinforced self-compacting concrete (SFRSCC) to manufacture lightweight panels for building facades.

Analytical models were proposed to simulate the monotonic and cyclic compressive stress-strain curves registered in experimental tests carried out with SCC reinforced with 45 kg/m^3 of hooked ends steel fibres.

Three point notched SFRSCC beams were tested according to the recommendations of RILEM TC 162-TDF at five distinct ages to assess the flexural tensile behaviour of the developed SFRSCC (30 kg/m^3 of fibres). The limit of proportionality, F_L, increased with the SFRSCC age, as well as the maximum load and the energy absorption capacity.

The benefits of fibre reinforcement were also visible in panel prototypes of redundant number of supports and failing in bending. The maximum load was significantly larger than the load at matrix crack initiation, and this load was practically maintained up to a panel central deflection of about 5 mm.

A real scale SFRSCC panel was fabricated under the real production conditions of the precasting company associated to this project, in order to verify if laboratory process used in the manufacture of the developed SFRSCC could be directly applied in an industrial environment. The tested panel resisted to its own weight and to a live load of 1.77 kN/m^2. This indicates that the developed panel system has structural requisites to support the internal forces due to the most unfavourable load conditions: wind and demoulding.

Acknowledgements

The study reported in this paper is part of the research program *PABERPRO – Conception and implementation of production system of lightweight steel fibre reinforced self-compacting concrete panels"* supported by Program POCI 2010 – IDEIA, Project nº 13-05-04-FDR-00007, contract reference ADI/2007/V4.1/0049. This project involves the Companies PREGAIA and CIVITEST, and the University of Minho. The authors wish to acknowledge the materials generously supplied by Bekaert (fibres), SECIL (cement), Degussa (superplasticizer), and Comital (limestone filler).

Notation

C	=	cement
CG	=	crushed granite
CS	=	coarse river sand
E_c	=	concrete elasticity modulus
E_{ci}	=	concrete tangent elasticity modulus, according to CEB-FIP Model Code 1993
E_{c1}	=	concrete secant elasticity modulus, according to CEB-FIP Model Code 1993
F_L	=	load at the limit of proportionality for three point notched beams flexural tests
FS	=	fine sand
G_f	=	mode I fracture energy
G_f^{III}	=	mode III fracture energy
LF	=	limestone filler
SCC	=	self compacting concrete
SFRC	=	steel fibre reinforced concrete
SFRSCC	=	steel fibre reinforced self compacting concrete
s_f	=	fibre-matrix slip
SP	=	superplasticizer
T_{50}	=	time to reach a spread diameter of 500 mm on the spread flow test
W	=	water
d_f	=	steel fibre diameter
f_{ct}	=	concrete tensile strength
h_{sp}	=	midspan section net depth at three point notched beams flexural test
l_b	=	crack band width
l_f	=	steel fibre length
s	=	total spread measured on the spread flow test
ε_n^{cr}	=	crack normal strain
ε_{c1}	=	strain at concrete compressive strength
ξ_i	=	fracture parameters used to define the tri-linear stress-strain softening diagram

σ_{ci}^{r} = compressive stress recorded at the ith scan reading in an experimental test

σ_{ci}^{c} = compressive stress obtained according to the analytical model proposed in the present work

σ_{n}^{cr} = crack normal stress

τ_{f} = fibre-matrix bond stress

1

References

ASTM C 39 - 96. (1996). "Standard test method for compressive strength of cylindrical concrete specimens." Annual book of ASTM Standards, 04.02: 18–22.

ASTM C 469 – 94. (1994). "Standard test method for static modulus of elasticity and poisson's ratio of concrete in compression." Annual book of ASTM Standards, 04.02: 238–41.

Barros, J.A.O. *et al.* (2005). "PABERFIA- Lightweight sandwich panels in steel fiber reinforced self compacting concrete." Technical Report 05-DEC/E-29, Dep. Civil Eng., School Eng. University of Minho, 63 pp.

Barros, J.A.O.; Figueiras, J.A., "Flexural behavior of steel fiber reinforced concrete: testing and modelling", Journal of Materials in Civil Engineering, ASCE, 11(4), p. 331-339, 1999.

CEB-FIP Model Code 1990. (1993), "Design Code." Comite Euro-International du Béton, Bulletin d'Information nº 213/214, 437 pp.

EFNARC (2002), "Specification and Guidelines for Self-Compacting Concrete." ISBN 0 9539733 4 4, 32 pp.

EN197-1:2000 (2000). "Cement. Composition, specifications and conformity criteria for low heat common cements." ISBN: 058036456 9, 52pp.

Okamura, H., Maekawa, K., "Nonlinear analysis and constitutive models of reinforced concrete." Gihodo-Shuppan Press, Tokyo, Japan, 1991

Okamura, H. (1997). "Ferguson Lecture for 1996: Self-compacting high-performance concrete." Concrete International, ACI 19(7), 50-4.

Pereira, E.N.B. (2006), "Steel Fibre Reinforced Self-compacting Concrete: from material to mechanical behaviour", dissertation for Pedagogical and Scientific Aptitude Proofs, Department Civil Engineering, University of Minho, 188 pp, <http://www.civil.uminho.pt/composites>

Poppe, A. and Shutter, G. D. (2005). "Cement hydration in the presence of high filler contents." Cement and Concrete Research, 35, 2290–2299.

RILEM TC 14-CPC8 (1975). "Modulus of elasticity of concrete in compression: final recommendation." Materials and Structures, 6(30), 25–27.

Vandewalle *et al.* (2002). "Test and design methods for steel fibre reinforced concrete - Final Recommendation." Materials and Structures 35(253), 579-582.

Robins, P, Austin, S., and Jones, P. (2002). "Pull-out behaviour of hooked steel fibres." Materials and Structures, 35(251), 434-442.

Rots, J.G. (1988). "Computational modeling of concrete fracture." PhD Thesis, Delft University of Technology.

Wang, C.Z.; Guo, Z.H.; Zhang X.Q., “Experimental investigation of the complete stress-strain curves of concrete under cyclic loading”, US/PRC Workshop on Seismic Analysis and Design of Reinforced Structures, Ann Arbor, Michigan, USA, 1981.

TABLE CAPTIONS

Table 1. SFRSCC compositions per m^3 of concrete.

Table 1. SFRSCC compositions per m^3 of concrete

Composition nº	*Paste Volume* [%]	*C* [kg/m^3]	*LF* [kg/m^3]	*W* [kg/m^3]	*SP* [kg/m^3]	*FS* [kg/m^3]	*CS* [kg/m^3]	*CG* [kg/m^3]	*Fibers* [kg/m^3]	*SCC requirements*
1	34	359.4	308.1	97.0	7.1	172.2	859.2	698.4	30	*s* = 720 mm T_{50}=3.5 sec
2	38	401.7	344.3	117.3	7.7	178.3	668.1	600.0	45	*s* = 730 mm T_{50}=7 sec T20=1 sec T40=2 sec H2/H1=0.89

FIGURE CAPTIONS

Fig. 1. Compression stress-strain relationship from specimens of distinct ages.

Fig. 2. Evolution with age of: (a) average compressive strength and (b) average elasticity modulus.

Fig. 3. Typical cyclic versus monotonic stress-strain relationship obtained the in experimental program: (a) Cyl9, (b) Cyl10 specimens.

Fig. 4. Experimental and analytical stress-strain curve for monotonic compression tests.

Fig. 5. Cyclic hysteretic model for SFRSCC.

Fig. 6. Experimental and analytical stress-strain curve for cyclic compression tests.

Fig. 7. Average load-deflection curves for specimens of distinct ages: (a) for a deflection up to 0.5 mm, and (b) for a deflection up to 3.1 mm.

Fig. 8. Punching test on panel prototype: (a) test setup, and (b) load-deflection experimental and numerical results.

Fig. 9. Flexural test on panel prototype: (a) test setup, and (b) load-deflection experimental results.

Fig. 10: Panel geometry (dimensions in mm): thickness = 110mm, total vol.=0.882 m^3, Lightweight=0.36 m^3, vol. to cast=0.522 m^3, approximated weight = 1305 kg.

Fig. 11. Setup of the loading test (dimensions in mm)

Fig. 12. Final view of the panel, loaded with 33 concrete plates

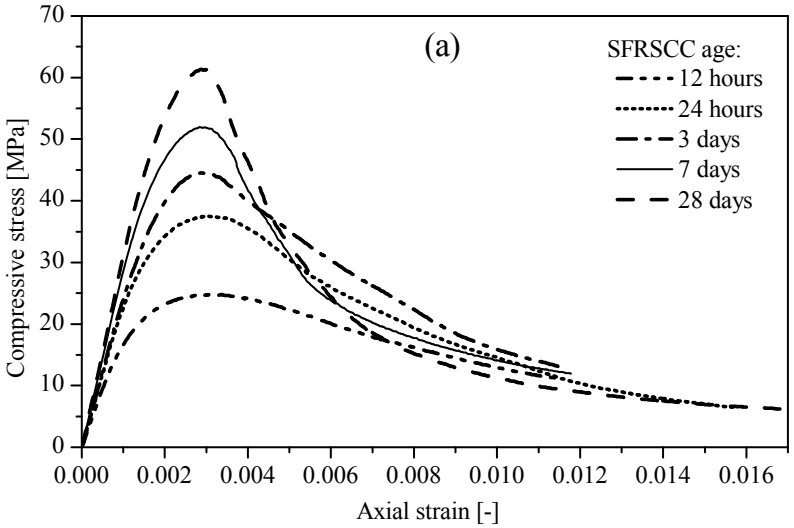

Fig. 1. Compression stress-strain relationship from specimens of distinct ages.

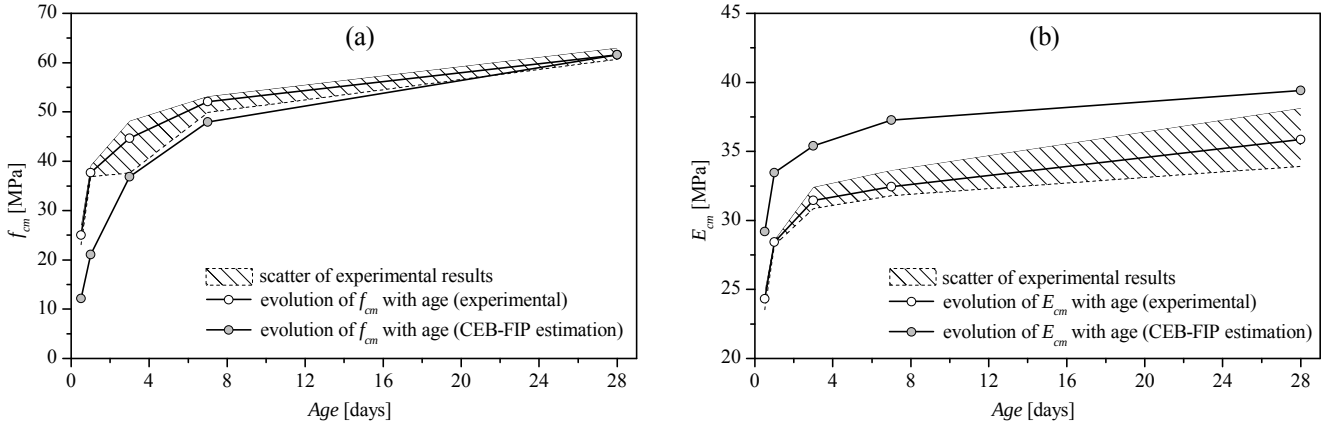

Fig. 2. Evolution with age of: (a) average compressive strength and (b) average elasticity modulus.

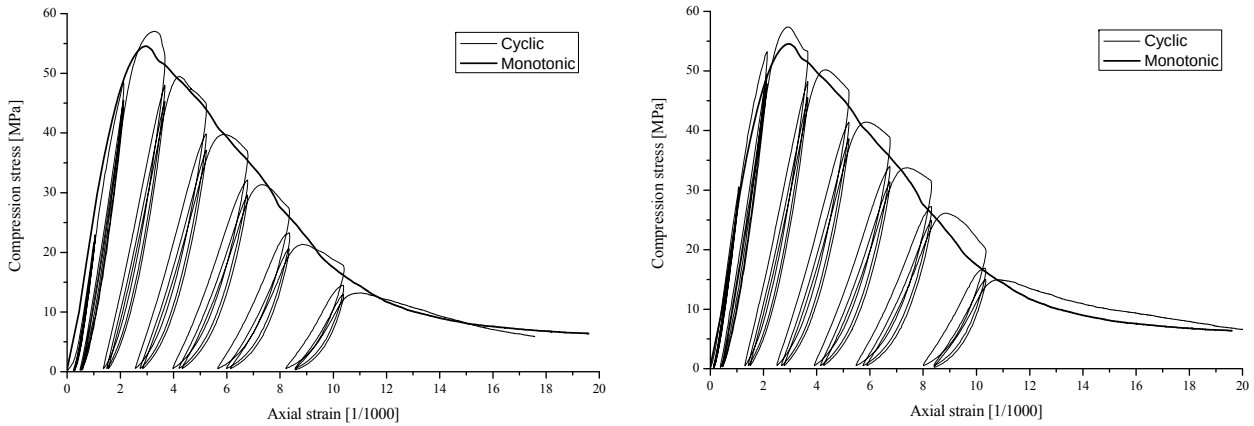

(a) (b)

Fig. 3. Typical cyclic versus monotonic stress-strain relationship obtained the in experimental program: (a) Cyl9, (b) Cyl10 specimens.

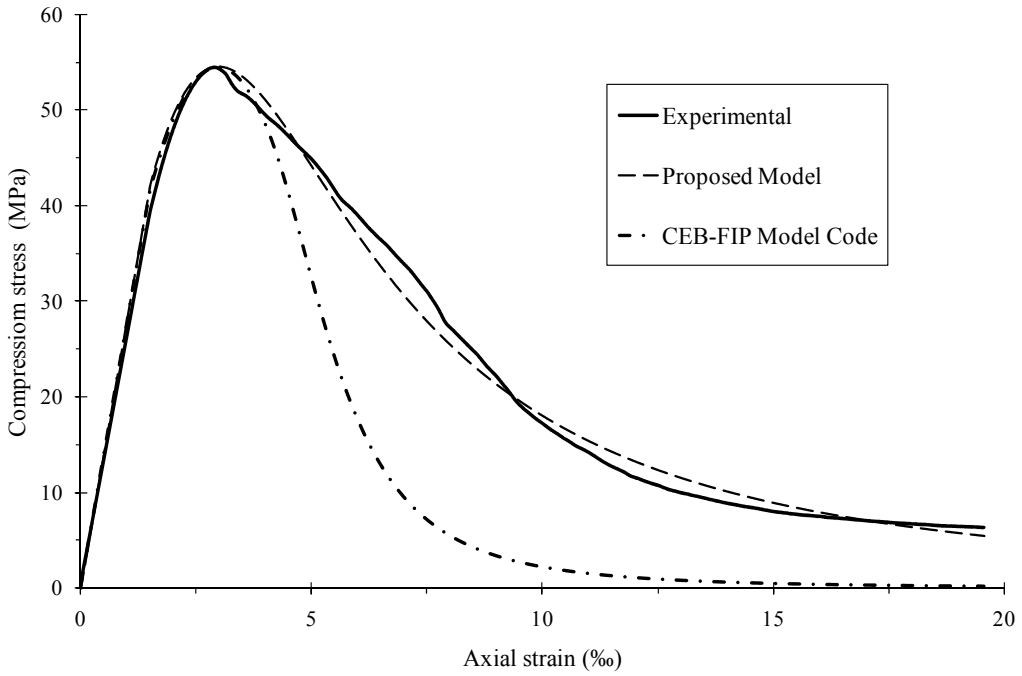

Fig. 4. Experimental and analytical stress-strain curve for monotonic compression tests.

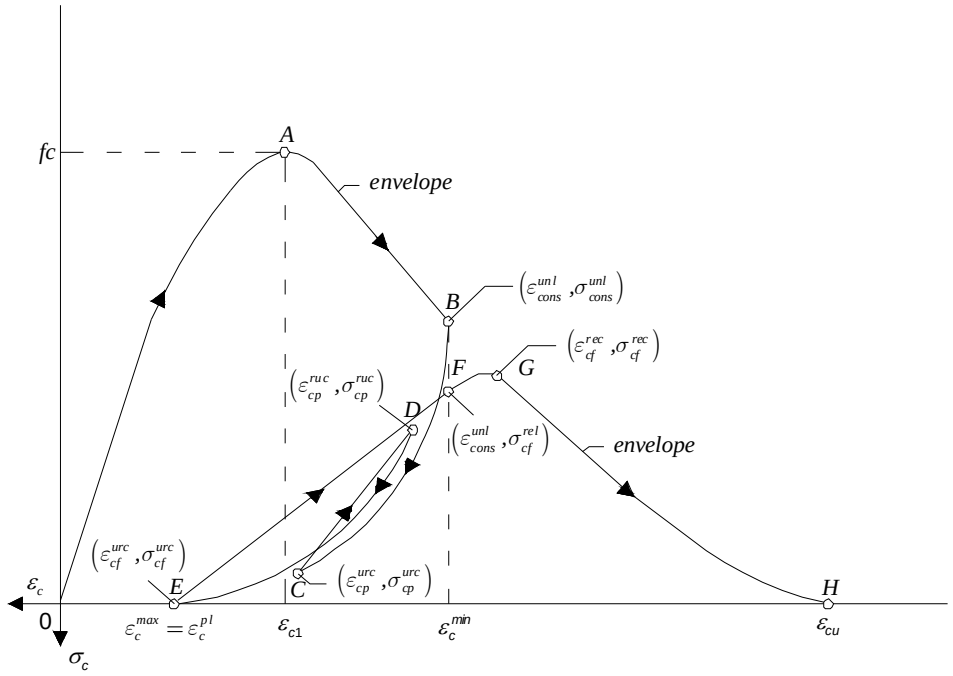

Fig. 5. Cyclic hysteretic model for SFRSCC.

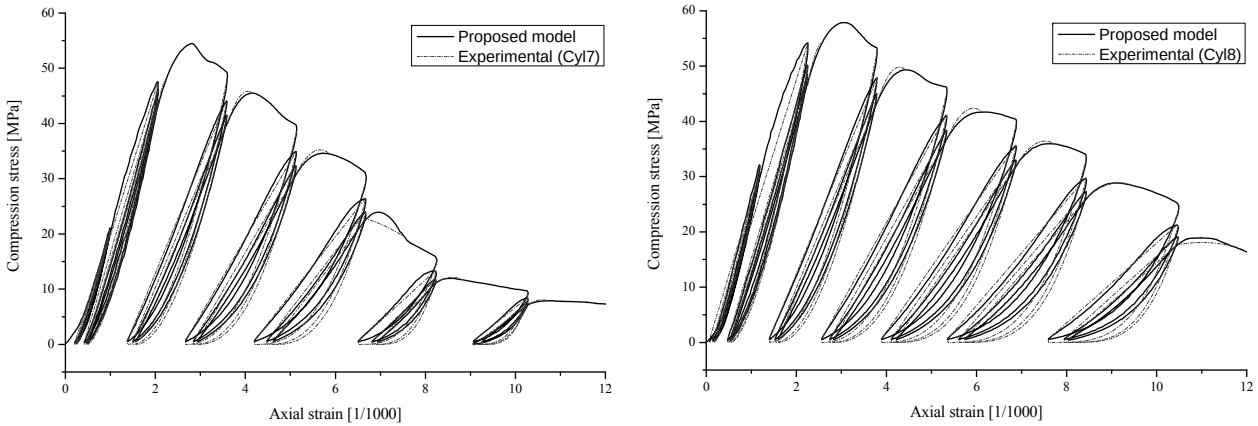

(a) (b)

Fig. 6. Experimental and analytical stress-strain curve for cyclic compression tests: (a) Cyl7, (b) Cyl8 specimens

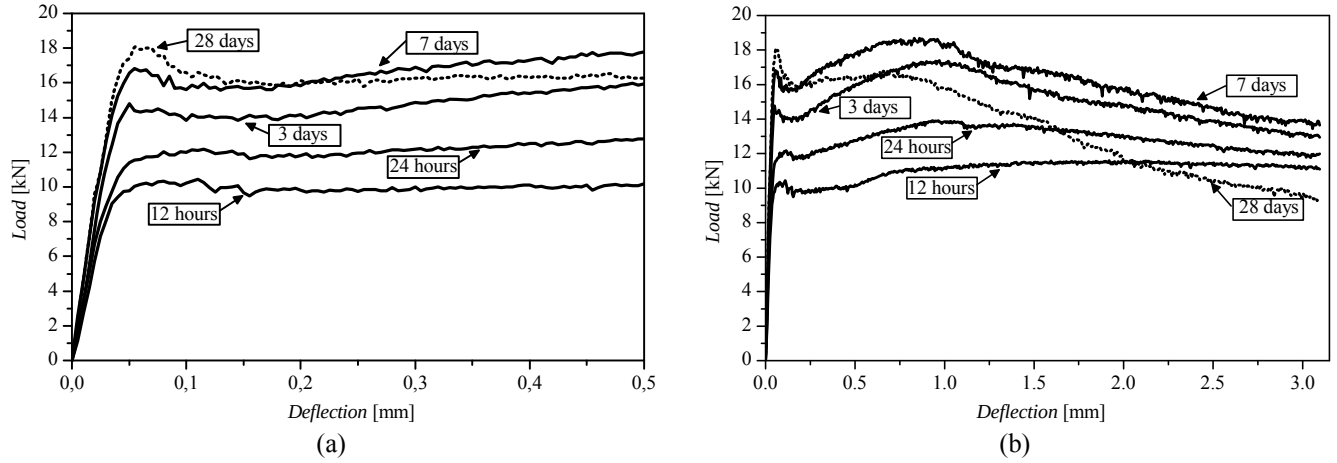

Fig. 7. Average load-deflection curves for specimens of distinct ages: (a) for a deflection up to 0.5 mm, and (b) for a deflection up to 3.1 mm.

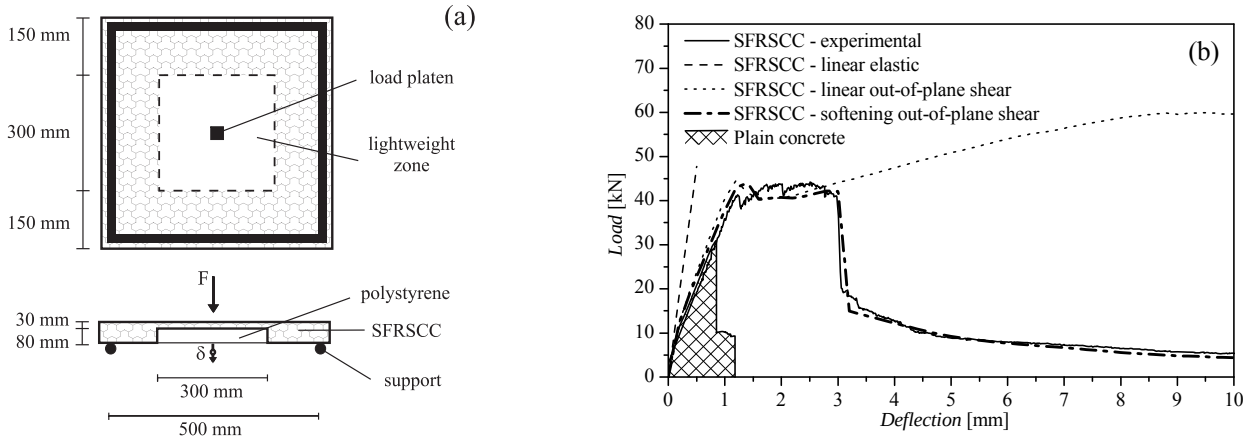

Fig. 8. Punching test on panel prototype: (a) test setup, and (b) load-deflection experimental and numerical results.

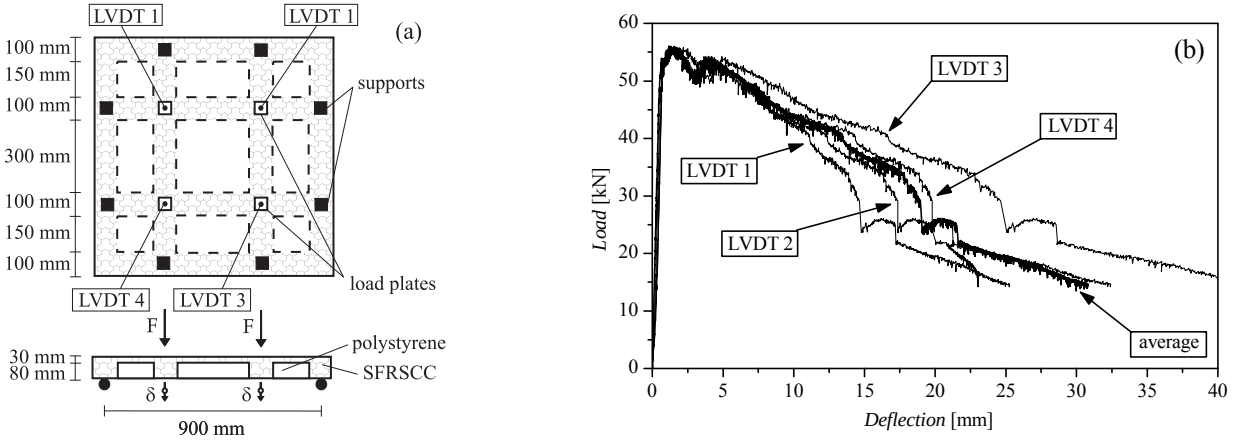

Fig. 9. Flexural test on panel prototype: (a) test setup, and (b) load-deflection experimental results.

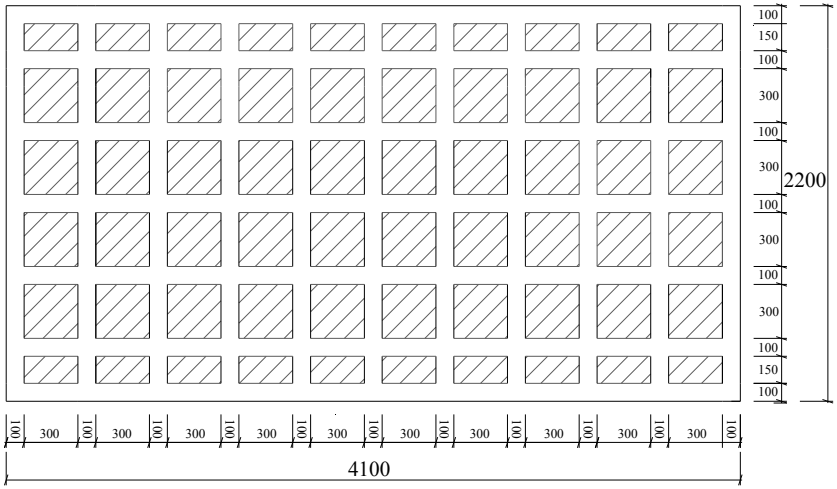

Fig. 10: Panel geometry (dimensions in mm): thickness = 110mm, total vol.=0.882 m^3, Lightweight=0.36 m^3, vol. to cast=0.522 m^3, approximated weight = 1305 kg.

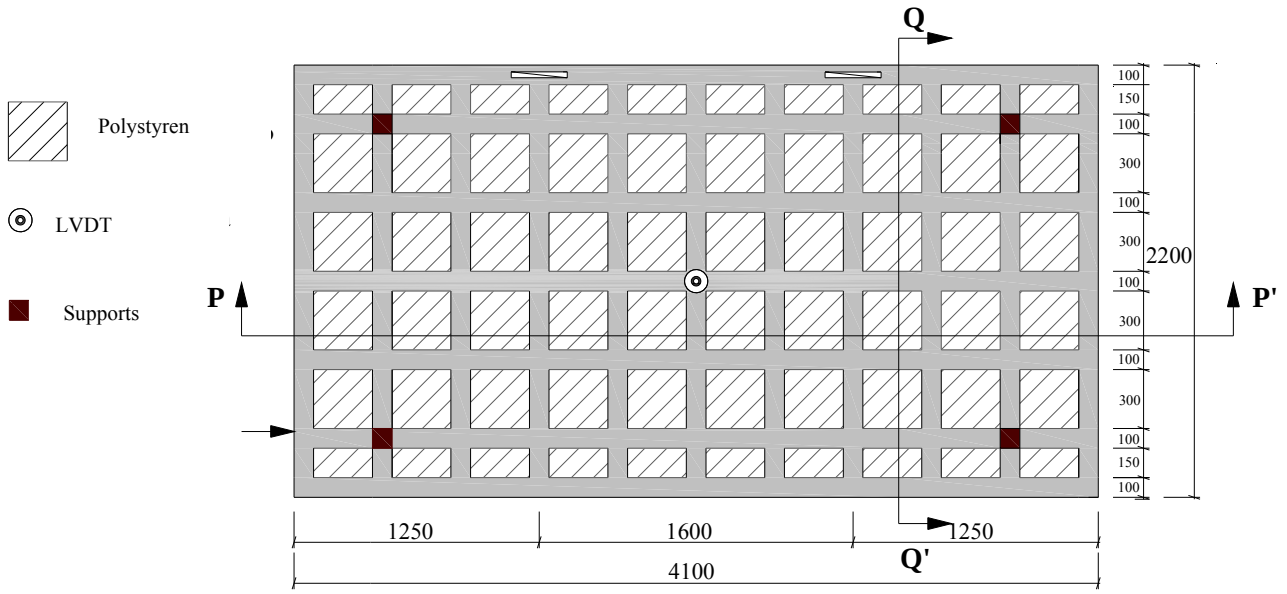

Fig. 11. Setup of the loading test (dimensions in mm)

Fig. 12. Final view of the panel, loaded with 33 concrete plates.